RSC Advances

ROYAL SOCIETY OF CHEMISTRY

www.rsc.org/advances

RSC Advances

ARTICLE

In Situ Preparation of MOF-derived Magnetic Carbonaceous Catalyst for Visible-Light-Driven Hydrogen Evolution

Received 00th January 20xx,
Accepted 00th January 20xx

DOI: 10.1039/x0xx00000x

www.rsc.org/

Jing-Yin Xu,[a,†] Xin-Ping Zhai,[a,†] Lin-Feng Gao,[a] Peng Chen,[b] Min Zhao,[a] Hong-Bin Yang,[a] Deng-Feng Cao,[a] Qiang Wang*[a] and Hao-Li Zhang *[a]

MOFs (Metal–Organic Frameworks) have emerged as a novel photocatalyst for water reduction but are frequently plagued by their instability when exposed to moist and strongly acidic or alkaline reaction environment. Herein we employed volatile Fe-based MOFs in alkaline solution as precursors to evolve into magnetic carbonaceous photocatalys *in situ,* which demonstrated highly efficient visible-light-driven hydrogen evolution (~125 μmol H_2 produced within 6 h using 5 mg MOFs precursors) with a quantum efficiency of 1.8% even in the absence of noble metal cocatalyst, indicative of a possible photocatalytic system containing only earth-abundant elements for long-term conversion of solar light into hydrogen energy. The catalyst exhibited an apparent stoichiometric formula of $FeO_{3.3}C_{0.2}H_{1.0}$ and was determined to be essentially carbon-metal oxides/oxyhydroxides composite. Laser photolysis and electrochemical measurement were performed to picture the fundamental multistep electron transfer processes during water reduction, which opens a strategy for the rationally design of MOF-derived catalyst to highly raise H_2 evolution efficiency.

Introduction

Metal-organic frameworks (MOFs), a class of hybrid materials built from the coordination of limitless choice of metal ions or clusters with organic ligands,[1-4] have exhibited intrinsically ordered three-dimensional (3D) structures that give rise to a myriad of potential applications such as gas adsorption and storage,[5-8] sensing,[9, 10] catalysis,[6, 11-13] separation,[14, 15] and nonlinear optical devices.[16, 17] More recently, the employment of MOFs as precursors/templates for the fabrication of other functional materials have received mounting attention.[18, 19] Under appropriate experimental conditions such as thermolysis, MOFs are potentially capable of forming porous carbon materials, carbon–metal/metal oxide hybrids, micro/nanostructured metal oxides, etc., owing to their highly ordered porous structures constructed from regular arrangement of metal nodes and abundant organic struts.[18] The strategy expands the potential and functionality of MOFs, compensating their usual instability from exposure to moisture, high temperature, chemical reagents such as strong acid or alkali. As a result, a sizeable amount of MOF-derived functional materials have emerged as promising novel challengers in catalysis, lithium-ion batteries, capacitors, electrode, fuel cell applications and so on. [18] However, to date MOF-derived functional materials for hydrogen evolution via water reduction is much less reported.

Inspired by the natural hydrogenases mimics containing active site of Fe_2S_2 cluster that have been intensively investigated for photocatalytic H_2 production,[20, 21] herein we developed MOF-derived carbon-metal oxides/oxyhydroxides composite *in situ* for visible-light-driven water reduction. MIL-101(Fe) is a MOF embedded with Fe-oxo metallic clusters, but is notoriously unstable in basic solution. However, through a mild *in situ* carbonization process, MIL-101(Fe) can serve as suitable precursors to be decomposed into micro/nano structured carbon–metal oxides/oxyhydroxides composite. This method bypassed thermolysis of the MOF precursors at high temperature and is rather facile and low-cost, indicative potential for large-scale fabrication. Moreover, the as-prepared carbonaceous catalyst is strongly magnetic and thus easily recoverable, one additional merit favored in photocatalytic application.

Indeed, the as-prepared carbon–metal oxides/oxyhydroxides composite acted as highly efficient catalyst for hydrogen evolution via water reduction, surpassing many of those previously reported H_2 evolution performance based on MOF structures. It is noteworthy that even without the presence of noble metal cocatalyst, the catalysts are capable of attaining high H_2 yield, indicative of a possible photocatalytic system containing only earth-abundant elements for long-term conversion of solar light into hydrogen energy. Laser photolysis and electrochemical measurements were employed to unravel their roles in H_2 production, which

[a] State Key Laboratory of Applied Organic Chemistry (SKLAOC), Key Laboratory of Nonferrous Metal Chemistry and Resources Utilization of Gansu Province, College of Chemistry and Chemical Engineering, Key Laboratory of Special Function Materials and Structure Design, Ministry of Education, Lanzhou University, Lanzhou, 730000, China *Corresponding authors. E-mail: qiangwang@lzu.edu.cn (Qiang Wang), haoli.zhang@lzu.edu.cn (Hao-Li Zhang)
[b] School of Pharmacy, Lanzhou University, Lanzhou, 730020, China
† The authors equally contributed to the manuscript. Electronic Supplementary Information (ESI) available: Figure S1-S6, Equations 1-3, Table S1. See DOI: 10.1039/x0xx00000x

pictured the fundamental multistep electron transfer processes during water reduction, open a strategy for the rational design of MOF-derived catalyst to highly raise H_2 evolution efficiency, and the Fe-based, environmental-friendly catalysts with a facile and scaled-up synthesis may eventually enable sustainable artificial photosynthesis and tackle the urgent energy issues facing the world.

Experimental

Materials

1,4-benzenedicarboxylic acid (BDC) was purchased from Tianjin GuangFu Technology Development Co. Ltd. Iron(III) chloride hexahydrate ($FeCl_3 \bullet 6H_2O$) was obtained from Tianjin Kaitong Chemical Co. Ltd. Sodium sulfate (Na_2SO_4) was obtained from Tianjin Shengmiao Chemical Co. Ltd. Eosin Y alcohol soluble (EY) was from Aladdin Chemistry Co. Ltd. Triethylamine (TEA) and N,N-dimethylformamide (DMF, dried), ethanol (EtOH, dried), acetonitrile (MeCN), acetone was purchased from Rionlon Bohua (Tianjin) Pharmaceutical& Chemical Co. Ltd. Deuterium oxide (D_2O, Qingdao Tenglong Weibo, 99.9% D). All solvents and chemicals were used without any further purification except for DMF and EtOH, which were dried with CaH_2 and Na and distilled under reduced pressure. Deionized water (resistivity: 18.3 MΩ•cm) was used to prepare aqueous solution throughout the experiment unless otherwise specified.

Syntheses of MIL-101(Fe) Precursor

The synthesis of size and morphology controlled crystals was accomplished following modified procedures as described in literatures.[22-24] In a typical synthesis procedure, 0.206 g (1.24 mmol) of BDC and 0.675 g (2.45 mmol) of $FeCl_3 \cdot 6H_2O$ were dissolved in 15 mL of DMF. The mixture was then introduced into a 50 mL Teflon-lined microwave vessel and sealed. The reaction was then rapidly heated to 110 °C at 400 watt microwave irradiation, and was held at this temperature for 10 minutes (PreeKem WX-4000 microwave digestion system, Shanghai). After cooling to room temperature, the particles were isolated by centrifuging, and were washed with DMF and ethanol.

MOF-derived Catalyst *In Situ* for Hydrogen Evolution

The as-synthesized MIL-101(Fe) of 5 mg was added to the acetonitrile/water solution in a 25-mL round-bottom flask, sealed with a silicone stopper, degassed, flushed with dry nitrogen, and sonicated in dark for ~1-2 min to ensure a uniform mixture. Photocatalytic hydrogen evolution experiments were performed by irradiating the solution under continuous stirring in the presence of Eosin Y (EY) and triethylamine (TEA) using a white-light LED (light spectrum: 400-750 nm; energy density: 13.7 mW/cm^2 at a distance of 6 cm) at room temperature. Thus the MOF-derived catalyst was synthesized *in situ* and the produced hydrogen was detected by a calibrated Varian GC-3380 Gas Chromatograph with a thermal conductivity detector and nitrogen as the carrier gas. For a repeated photocatalytic cycle measurement, the catalyst was first separated via centrifugation and thereafter the same procedure as the first H_2 collection cycle was carried out with supplement of the same amount of reaction reagents, *i.e.*, solvent, EY and TEA. The optimized reaction conditions are used for H_2 production with suitable amount of catalyst in acetonitrile/water (v/v=1:1) solution in the presence of EY (8.0×10^{-4} M) and TEA (10 % v/v), at a pH value of 10.0 adjusted by hydrochloric acid. To carry out the deuteration experiments, deuterium oxide was used to replace water, and the produced gas mixture was analyzed by Gas chromatograph/mass spectrometry (GC/MS) on a SHIMADZU GCMS-QP2010 SE instrument. After hydrogen evolution measurement, the catalyst was separated via centrifugation for characterization.

Characterization

Spectroscopic measurement

The FT-IR spectra were recorded using a VERTEX 70V/80V Fourier transformed infrared spectrometer (Bruker, Germany) by means of the KBr pellet technique. Raman spectra were measured with a Renishaw in via Raman Microscope System at the excitation of 785 nm. The UV/VIS diffuse reflectance spectra were obtained on a Cary 5000 UV-Vis-NIR spectrometer (Agilent Technologies) equipped with Labsphere integrating over the spectral range of 190-900 nm. Laser photolysis experiments were performed on a LP920 (Edinburgh Instrument) transient absorption spectrometer available with kinetic (PMT) and spectral (ICCD) dual detection modes. The OPO laser (Opolette HE 355 LD UVDM, Optotek Inc.) with output wavelength from 236 nm-2400 nm was employed as the excitation source (525 nm for this measurement) and the samples were purged with nitrogen to remove oxygen in the solution before measurements. Sample conditions: MOF precursor (5 mg); EY (1.0×10^{-5} M); TEA (10% v/v); all in acetonitrile/water (v/v=1:1) solution at a pH value of 10.

Other characterizations

The size and morphology of samples were characterized using field-emission scanning electron microscopy (FE-SEM, Hitachi S4800) at an accelerating voltage of 5.0 kV. The samples for SEM analysis were prepared by dripping an ethanol solution of crystals onto silicon wafer and dried under 60°C. The TEM micrographs were obtained using a Tecnai G^2 F30 Field Emission Transmission Electron Microscope at an operating voltage of 300 kV. Samples were dispersed onto holey carbon grids with the evaporation of excess solvent. Powder X-ray diffraction (XRD) patterns of the products were recorded on a Panalypical X' Pert PRO diffractometer using Cu K α X-rays between 2.5° and 60°. X-ray photoelectron spectroscopy (XPS) was performed on AXIS Ultra. Nitrogen adsorption-desorption isotherms were measured on a Micromeritics ASAP 2020 M at 77 K. Thermogravimetric (TGA) curves were obtained on a STA PT1600 from room temperature to 800 ℃ under nitrogen atmosphere. The magnetization measurements were carried out at ambient condition on a LakeShore 735 Vibrating Sample

Magnetometer. Elementary analysis was performed by using a Vario EL cube and Fe element content was determined via inductively coupled plasma atomic emission spectroscopy (ICP-AES) on IRIS ER/S.

Electrochemical measurements

CHI 660b electrochemical workstation (Shanghai Chenhua) was used to perform Mott-Schottky analysis of samples (coated on ITO as working electrode, Pt as counter electrode and 0.5 M Na_2SO_4 as electrolyte) at frequencies of 10 KHz.

Results and discussion

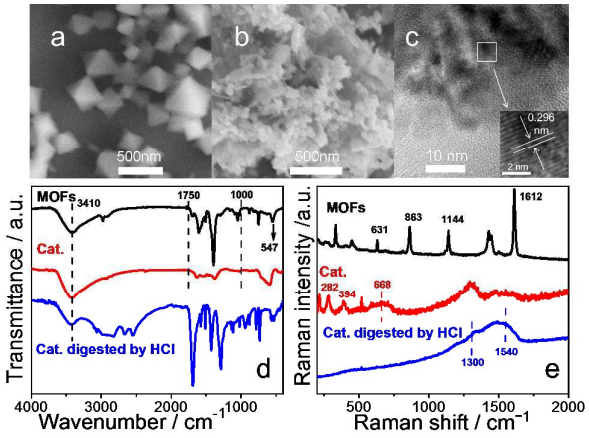

Figure 1. SEM images of (a) MIL-101(Fe) ("MOFs"), (b) the MOF-derived catalyst ("Cat.") and HRTEM image of the Cat. (c). (d) FTIR and (e) Raman spectra of MOFs, Cat. and the catalyst after digested by concentrated HCl to remove iron element ("Cat. digested by HCl").

MIL-101(Fe) precursors were prepared following a modified route, [22-24] where $FeCl_3 \cdot 6H_2O$ and terephthalic acid (BDC) were heated with the assistance of microwave in pure DMF. The precursors were then directly applied for photocatalytic reactions, which would be rapidly decomposed into the catalyst (Cat.) *in situ* subject to alkaline media and visible–light irradiation. As displayed by the Scanning electron microscopy (SEM) images (Figure 1a), MIL-101(Fe) particles exhibit an octahedron morphology and an average diameter of ~500 nm, consistent with previous report.[24] By contrast, the as-synthesized Cat. after separation showed amorphous and porous microstructures (Figure 1b). The weight percentage of iron element was determined to be 49.6% by inductively coupled plasma atomic emission spectroscopy (ICP-AES). In combination with the weight ratio of 2.6%, 1.0%, 46.8% for C, H and O, respectively via elementary analysis, the stoichiometric formula of the carbon/metal or metal oxide composite was tentatively deduced to be $FeO_{3.3}C_{0.2}H_{1.0}$. To disentangle the exact composition of the catalyst is challenging, as under the synthesis conditions, *i.e.*, alkaline medium, light irradiation and absence of high temperature thermolysis, the Fe-based MOF precursors would experience complicated reactions and evolve into copious combinations between carbon and the extremely rich iron oxides/ oxyhydroxides family, Fe_2O_3 of α, γ phases, Fe_3O_4, FeOOH of α, β, γ phases, to name a few. Therefore, in the following work, we tried various characterization techniques to provide information on the composition of the catalyst.

One type of lattice fringes with the lattice spacings of 0.296 nm was shown in the High Resolution Transmission electron microscope (HRTEM) image of the Cat. (Figure 1c), probably corresponding to the (220) plane of γ-Fe_2O_3 nanoparticles.[25] FTIR, Raman spectroscopic measurements and XRD patterns were further employed to confirm the generation of the Cat. via MIL-101(Fe) precursors (Figure 1d, e, respectively). Clearly, the FTIR spectrum of MIL-101(Fe) exhibited typical vibrational bands in the region of 1000–1750 cm^{-1} for the carboxylic functional groups,[26, 27] which disappeared or transformed in the spectrum of the Cat.. Specifically, 1380-1630 cm^{-1} were tentatively attributed to the deformation vibrations of H-O-H of iron oxyhydroides (FeOOH) species contained in the Cat..[28] The band at 547 cm^{-1} of MIL-101(Fe) was attributed to Fe–O–C bending vibrations,[29] which however turned into the Fe–O vibration peak of 460 cm^{-1} for the Cat. and vanished after the Cat. was digested by concentrated HCl to remove iron element (**"**Cat. digested by HCl**"**). Both MOFs and the Cat. showed broad band centering around 3410 cm^{-1} due to stretching vibrations of hydroxyl groups. Raman spectra of the three materials were also distinctly different. For MIL-101(Fe), the peak at 466 cm^{-1} could be assigned to the Fe-O vibration.[27] The bands at 631, 863 and 1144 cm^{-1} were attributed to the deformation vibrations of the aromatic -CH groups. The symmetric stretch of the carboxylate groups and the C=C vibration could be found between 1370 and 1470 cm^{-1}. The band with the highest intensity (1612 cm^{-1}) was assigned to the asymmetric stretch of the carboxylate group. The Raman bands of the Cat., however implied a coexistence of iron oxides/oxyhydroxides in different phases. The band centering around 668 cm^{-1} was ascribed to either γ-Fe_2O_3 or Fe_3O_4. [30, 31] The bands at 216 and 394 cm^{-1} were considered characteristics of α-Fe_2O_3, [31, 32] whereas the peaks at 282, 588, and 668 cm^{-1} were typical bands of Fe_3O_4, and 282, 394, 1300 cm^{-1} could be also from α-FeOOH.[30] The bands around 1300 and 1500 cm^{-1} were complicated, which could stem from γ-Fe_2O_3, α-FeOOH and carbon. Accordingly, by examining the Raman shifts of the Cat. digested by HCl, it was found that the typical bands for the metal oxides/oxyhydroxides vanished, and the residual broad bands at 1300 and 1540 cm^{-1} were expected to correspond to disordered amorphous carbon (D band) and graphite (G-band) respectively,[31, 33] indicative of the formation of amorphous carbon. Therefore based on the above discussions, γ-Fe_2O_3 and α-FeOOH could be the composites of the Cat.. α-Fe_2O_3 is the most thermodynamically stable phase among the iron oxides family and the formation of it usually requires high thermolysis temperature,[28] which contracts with our reaction condition.

Hence the appearance of typical Raman shifts of α-Fe_2O_3 may be induced by the laser during measurement, which could transform γ-Fe_2O_3, Fe_3O_4 or FeOOH species into α-Fe_2O_3.[30] Meanwhile, γ-Fe_2O_3 could be partially reduced to Fe_3O_4 during the *in situ* synthesis of the catalyst,[31, 33] which may account for certain characteristic Raman peaks of Fe_3O_4 in the spectra.

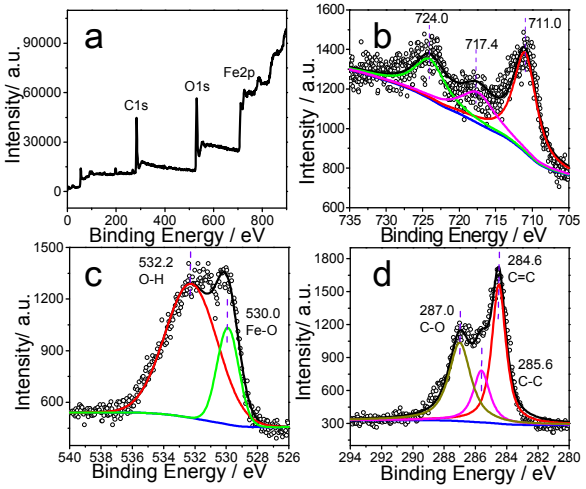

Figure 2. XPS spectra of the Cat.: (a) survey spectrum, and high-resolution (b) Fe 2p, (c) O 1s, (d) C 1s binding energy spectra.

Clearly, further evidence is required to ascertain the constitute of the Cat.. XRD patterns alone are hard to distinguish the iron oxide phases as α-Fe_2O_3 , γ-Fe_2O_3 and Fe_3O_4 possess resemble diffraction peaks.[32-34] Moreover, the measured XRD patterns of the Cat. showed no obvious peaks corresponding to crystalline phases of carbon or Fe phase in any form (Figure S1), but similar to that of amorphous FeOOH. The XRD patterns of Cat. digested by HCl in the absence of iron element implied amorphous carbon. Therefore, X-ray photoemission spectroscopy (XPS) was utilized to further investigate the chemical compositions and the electronic structures of the composite in order to discern the varied phases thereof.

Figure 2a indicate Fe, O and C peaks all exist in the survey XPS spectrum. Three characteristic peaks of Fe $2p_{3/2}$ at 711.0 eV, 717.4 eV and Fe $2p_{1/2}$ at 724.0 eV were shown in Figure 2b of the high resolution curve-fitted XPS spectrum. It is known Fe 2p core-level spectra of some iron oxides/oxyhydroxides, such as α-Fe_2O_3 , γ-Fe_2O_3 and α-FeOOH are very similar with each other although their crystal structures are distinct,[35, 36] and hence it is hard to identify them via XPS spectra. However, so called "shake-up" peaks sensitive to the electronic structure of iron oxides/oxyhydroxides are often employed as fingerprints to discern their different phases.[35] Herein the satellite peak at 717.4 eV is regarded as the evidence of the presence of Fe^{3+} and absence of Fe^{2+}, [31, 34, 37] implying Fe_3O_4 in the Cat. is rare even if it does exist. On the other hand, the O 1s spectrum decomposed with the Gaussian distribution in Figure 2c clearly showed the presence of Fe-O and O-H groups, with binding energies at 530.0 eV and 532.2 eV, respectively. According to previous literature,[36] the result suggested the presence of α-FeOOH and the existence of water was also possible. Meanwhile, the decomposed C 1s spectrum implied the existence of different carbon-containing functional groups, such as C=C, C-C, C-O, reflecting the electronic structures of carbon in the Cat. and was in agreement with aforementioned FTIR and Raman spectroscopic measurements.

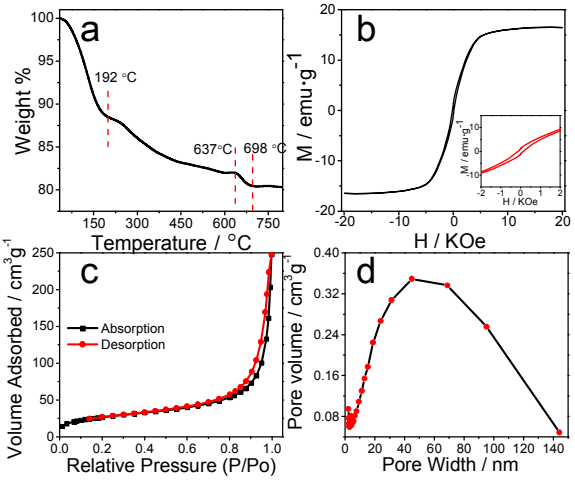

Figure 3. Thermogravimetric curve under nitrogen atmosphere (a), Magnetization curve at ambient condition (the inset is the enlarged part.) (b), N_2 adsorption/desorption isotherms (c) and pore size distribution measured at 77 K (d) of the Cat..

The composition of the catalyst is further analyzed by Thermogravimetric experiment (TGA). The TGA curve of the Cat. under N_2 atmosphere is shown in Figure 3a. The weight loss from 30 ℃ to 192 ℃ was attributed to the release of H_2O, the existence of which had been suggested by the above FTIR and XPS measurement. There are two weight loss steps in the temperature. The next weight loss up to 637 ℃ is expected stem from the decomposition of different phases of iron oxides/oxyhydroxides, mainly α-FeOOH.[38] The weight continues to lose at 637-698 ℃,which is ascribed to the oxidation of carbon phase in the catalyst, and the weight loss of ~1.5% is close to the carbon content of 2.6% of the catatlyst via element analysis. The weigh-loss process ceased after 698 ℃ while the heating continues until to the eventual 800 ℃. The weight of the stable residue was assigned as α-Fe_2O_3, accounting for a weight of ~80.4%, consistent with the ~49.6% of iron content measured by ICP-AES.

Magnetic feature is another way to effectively distinguish magnetic γ-Fe_2O_3 and Fe_3O_4 particles from weakly or none magnetic α-Fe_2O_3 and α-FeOOH.[28, 39] Figure 3b displayed the field-dependent magnetization curve of the Cat., where a hysteresis loop (see the inset) indicated its ferromagnetic characteristic. A saturation magnetization value of 16.5 emu g^{-1} at 20 T is large enough for the Cat. to undergo efficient magnetic separation with external magnetic field.[37] Combining with the above result, the observation further verified the γ-Fe_2O_3 constitute in the catalyst. In the end, nitrogen

adsorption-desorption isotherm measurement were carried out to determine the pore properties of the Cat.. Figure 3c indicated a typical IV isotherm reflecting porous materials with BET surface areas of 93.7 m^2/g, a value much less than that of its MOF precursor. Figure 3d showed a broad range of pore diameter distribution from 2 to 140 nm, and average pore size of ~16 nm, revealing the Cat. was a porous material mainly with mesopores. To sum up, the *in situ* generated magnetic carbonaceous catalyst from Fe-based MOFs exhibited an apparent stoichiometric formula of $FeO_{3.3}C_{0.2}H_{1.0}$, but is essentially carbon-metal oxides/oxyhydroxides composite, with features partially characteristic of amorphous carbon, γ-Fe_2O_3 and α-FeOOH. Additionally, note another possibility was O-containing organic groups (-OH, -CHO, -COOH, etc.) tethered carbon with ferric oxide. The multiple-component system has potentials of executing synergetic effects in a photocatalytic reaction.

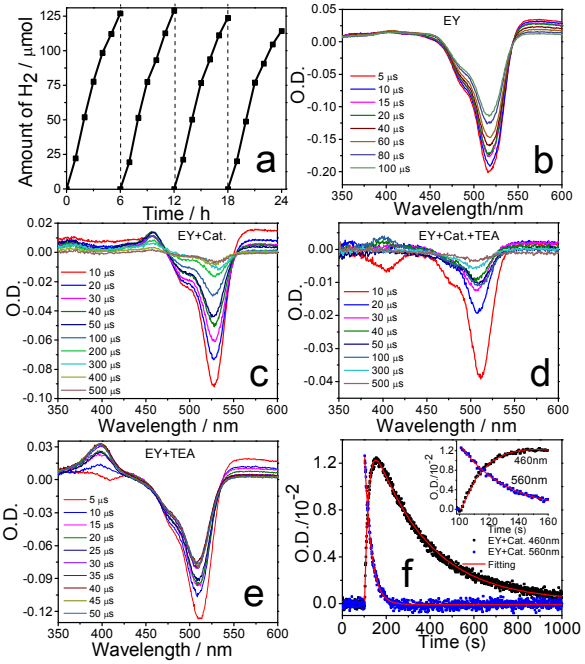

Figure 4. Rate of photocatalytic H_2 evolution using the *in situ* prepared Cat., 4 repeated cycles (a). Transient absorption spectra of EY (b), EY+Cat. mixture (c), EY+TEA mixture (d), EY+ Cat.+TEA mixture (e) and fitted decay curves for EY+Cat. mixture at 560 nm and 460 nm (f). The inset is the enlarged part for the very early time dynamics. The laser excitation wavelength is 525 nm.

The utility of our catalysts was then demonstrated for visible-light-driven hydrogen evolution. MOF-based photocatalysts with integrated visible-light-responsive organic linkers would be ideal for hydrogen production under solar light irradiation, which however frequently involves multistep organic synthesis procedures.[40, 41] Alternatively, considering current dye-sensitization photocatalytic system usually comprising of commercial photosensitizer and sacrificial reagent is rather mature and cost-effective,[42-44] we performed photochemical H_2 evolution experiments by irradiating the catalysts with a white-light LED in the presence of Eosin Y (EY, photosensitizer) and triethylamine (TEA) as sacrificial reagent in acetonitrile/water solution (v/v=1:1). Acetonitrile was used in the mixed solvent to improve the solubility of TEA and EY (ethanol soluble), which are not soluble well in pure water. This type of mixed solvent have been widely applied in previous photocatalytic water reduction system.[45, 46] The strategy could be a general way for photocatalytic water reduction via catalysts deficient in visible light response. Rates of photocatalytic H_2 evolution with MOF-derived catalyst were shown in Figure 4a. The visible-light-driven H_2 evolution via the Cat. is highly efficient, even in the absence of the frequently indispensable noble metal cocalalyst as in previous reports.[47, 48] Within 6 hours, the amount of H_2 produced was ~125 μmol with just 5 mg MOFs precursors, and the calculated Quantum Efficiency (QE) was 1.8% (see the section on QE calculation procedures in supporting information, and Figure S2). The Cat. also exhibited long durability and could be repeatedly used for several cycles without elemental content changes. The results emulated or surpassed those previously reported H_2 evolution performance based on MOF structures in any form, either using MOFs as photosensitizers, semiconducting photocatalysts, or simply support for loading Pt particles.[40, 43, 48-51] Control experiments indicated when neither the catalyst nor irradiation was present, H_2 was not produced, implying that both the catalyst and the light are indispensable for the photocatalytic process. Commercial iron oxide nanoparticles like Fe_2O_3, Fe_3O_4 also did not produce H_2. Likewise, individual components such as α-FeOOH also did not produce detectable hydrogen under the same reaction conditions. The result confirmed the multiple-component composite was not simply mixtures. It demonstrated synergetic effects in the photocatalytic reaction-the carbon content is low in the catalyst but may play crucial roles, and whether there is some special bonding between carbon and iron needs further exploration. Meanwhile, when deuterium oxide was used to replace water, the produced gas mixture analyzed by Gas chromatograph/mass spectrometry (GC/MS) proved a dominant presence of D_2 (Figure S3), strongly evidencing water was the origin for the hydrogen generated during the photocatalysis.[52, 53] In addition, although the catalyst exhibits considerable light response in the visible range as confirmed from diffuse reflection measurement in the following section, no detectable H_2 production would be observed without the assistance of the photosensitizer.

It is noteworthy that heterogeneous catalysts exhibited magnetic behaviors and can be conveniently recycled by an external magnet (Figure S4). Considering that isolation and reusability of one catalyst are crucial factors for industrial applications, the robustness and easy recyclability would endow the MOF-derived catalyst with great potential for practical use.

We also used other types of Fe-based MOFs as precursors to replace MIL-101(Fe) to investigate the impact of catalyst composition changes on the photoactivity. For instance, MIL-53(Fe)(Figure S5), which was prepared by using the same precursors of Iron(III) chloride hexahydrate and 1,4-

benzenedicarboxylic acid, gave a catalyst with a higher carbon content (weight ratio of 4.5%) than that of MIL-101(Fe)-derived catalyst. The H_2 evolution efficiency of this as-prepared catalyst was ~48 μmol gas produced within 5 h using 5 mg MOFs precursors, decreasing to less than half of that from MIL-101(Fe) derived catalyst under identical conditions. A systematic comparisons of H_2 evolution efficiency by catalysts derived from different precursors which therefore exhibited various elemental contents would be very interesting, and would be explored in separate work.

In order to disentangle the photocatalytic mechanism of the catalyst, we performed laser photolysis measurement to understand the dynamic processes during H_2 formation. In Figure 4b, the peak at 560 nm was attributed to the absorption of excited triplet state of EY ($^3EY^*$).[42, 54] Subsequently, $^3EY^*$ underwent one electron transfer to the Cat. and became a radical cation of $EY^{+\bullet}$, as evidenced by its typical absorption at 460 nm (Figure 4c),[42, 54] which is absent in the transient absorption spectra of sole EY. Fitting the absorption curve of $^3EY^*$ to a monoexponential decay equation gave one lifetime component of 31 μs (560 nm, Figure 4f), which is remarkably reduced compared with the 132 μs from sole EY (see supporting information for the fitting methods, and Table S1). Based on the expression of $k=1/\tau_{(cat.+EY)}-1/\tau_{EY}$, the electron transfer rate k from $^3EY^*$ to the Cat. was calculated to be 2.5×10^4 s^{-1} (Table S1).[42, 55] While the absorption decay curves of $EY^{+\bullet}$ (460 nm) followed a multiexponential decay and led to two lifetime components of 18 μs and 248 μs, respectively. The rapid rise of 18 μs corresponded to the formation time of $EY^{+\bullet}$, which occurred concomitantly with the decay of $^3EY^*$ of 31 μs (Figure 4f, inset), confirming the electron transfer from $^3EY^*$ to the Cat.. The second 248-μs component is attributed to the lifetime of $EY^{+\bullet}$, which thereafter will be regenerated if sacrificial donor exists in the system, as evidenced by the significantly quenched $EY^{+\bullet}$ absorption in Figure 4d in the presence of TEA. Control experiment had clearly showed that $^3EY^*$ was capable of acquiring electrons from TEA, indicated by the formation of $EY^{-\bullet}$ with a typical absorption band at 403 nm with a long lifetime over 6 ms when the EY and TEA mixture was photo excited (Figure 4e and Table S1).[42] Hence the entire photocatalytic system operate in the following cycle without intermittence: the catalyst attains electrons from EY (photosensitizer) for reduction of protons, and TEA (sacrificial reagent) on the other hand replenish electrons for EY to recover (Figure 4e).

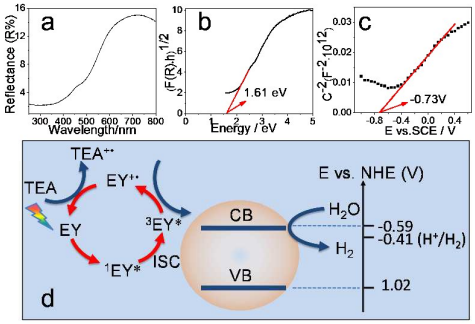

Figure 5. The UV/VIS diffuse reflectance spectra (a), corresponding Tauc plot (b), and Mott–Schottky plot in 0.5 M Na_2SO_4 aqueous solution (c) of the Cat.. Proposed H_2 production cycles photocatalyzed by the Cat. (d).

We further employed UV/VIS diffuse reflectance spectroscopy and electrochemical measurements to extract energy level information of the relevant parts in the photocatalytic system. From the diffuse-reflectance spectrum of the Cat. (Figure 5a), the optical absorption of the sample can be approximated via the Kubelka–Munk function of $F(R)=(1-R)^2/2R=\alpha/S$, where R is reflectance, α the absorption coefficient and S the scattering coefficient.[56-58] The Tauc plot for the Cat. was then drawn with a standard relationship of $(F(R)\bullet h\nu)^{1/2}=A(h\nu-E_g)$, where h is Plank constant, ν the frequency, A the constant and E_g the sample band gap.[49, 56-58] Extrapolate a straight-line of the linear part of the curve within the lowest energy region to $(F(R)\bullet h\nu)^{1/2}=0$ (Figure 5b), and then a band gap of 1.61 eV for the Cat. was obtained. In comparison, the band gap of MIL-101 (Fe) gave a value of 2.11 eV (Figure S6). We speculate that the narrower bandgap of the Cat. stemmed from its unique structure, which was in essence carbon-metal oxides/oxyhydroxides composite containing a considerable amount of amorphous carbon content.

Meanwhile, a positive slope of the Mott-Schottky (MS) plot indicated the Cat. was an n-type semiconductor (Figure 5c).[49] The Fermi level of the Cat. was determined to be -0.73 V vs. SCE (*i.e.*, -0.49 V vs. NHE), equal to its flat band potential. Consequently, the conduction band (CB) edge of the Cat. was estimated to be -0.59 V, ca. 0.10 V more negative than the flat band potential.[49] Compared with the LUMO level of EY (-1.05 V vs NHE),[59] CB edge of the Cat. is lower-lying, which would facilitate the electron transfer from EY to the Cat. and lead to an efficient charge separated state. The electron sequentially transfers to protons for a reduction to hydrogen as the CB edge of the Cat. is positioned above the reduction level for H_2.

Hence the entire photocatalytic H_2 evolution picture could be described by Figure 5d. Upon photoexcitation, EY is prone to undergo intersystem crossing from singlet state to more active triplet state under deoxygenized environment. As its LUMO level is higher than the CB band of the catalyst, one electron transfers to the latter, which sequentially relays to even lower energy level for proton reduction. Meanwhile, EY can be supplemented with electrons from the sacrificial donor to extend the self-sustaining cycle incessantly. Once any link of the chain is broken, for instance, replacement of the catalyst by other materials with inappropriate CB bands, the electron transfer will be terminated and consequently no hydrogen will be produced. Overall, the transient dynamic process and the energy level determined from the electrochemical measurement substantiate the proposed scenario.

Conclusions

In this study, we reported a magnetic carbonaceous catalyst decomposed from earth abundant Fe-based MOFs *in situ* for highly efficient visible-light-driven hydrogen evolution for the first time. With this general strategy, instable MOF

structures when exposed to moisture, thermal treatments, or chemical agents etc. however can be utilized as precursors to evolve into stable micro/nano materials. One striking result is high H_2 yield of the MOF-derived catalyst even in the absence of noble metal co-catalyst. The employment of earth-abundant elements as cost-effective substitute for Pt, Pd, Ru, Ir and Rh in photocatalytic water reduction renders the production of hydrogen energy more pragmatic. Additionally, various methods such as laser photolysis and electrochemical measurements were applied to thoroughly investigate the roles of the catalyst in H_2 production. Time-resolved spectra specifically provided unambiguous spectroscopic evidence on the transient species and the electron transfer dynamics during catalysis, providing new insights into the design of highly efficient catalyst for H_2 evolution from the perspective of photocatalytic dynamics.

Acknowledgements

This work is supported by National Basic Research Program of China (973 Program, No.2012CB933102), Gansu Province Science Foundation for Distinguished Young Scholars (Grant No. 1308RJDA014), Longyuan Support Project for Young Creative Talents (Grant No. GANZUTONGZI [2014] no.4), the Fundamental Research Funds for the Central Universities (lzujbky-2013-66), SRF for ROCS, SEM.

Notes and references

1. J. Kim, B. L. Chen, T. M. Reineke, H. L. Li, M. Eddaoudi, D. B. Moler, M. O'Keeffe and O. M. Yaghi, *J. Am. Chem. Soc.*, 2001, **123**, 8239-8247.
2. O. K. Farha and J. T. Hupp, *Acc. Chem. Res.*, 2010, **43**, 1166-1175.
3. W. Xuan, C. Zhu, Y. Liu and Y. Cui, *Chem. Soc. Rev.*, 2012, **41**, 1677-1695.
4. Q. L. Zhu and Q. Xu, *Chem. Soc. Rev.*, 2014, **43**, 5468-5512.
5. H. J. Lee, W. Cho, S. Jung and M. Oh, *Adv. Mater.*, 2009, **21**, 674-677.
6. Y. Y. Liu, Y. M. Yang, Q. L. Sun, Z. Y. Wang, B. B. Huang, Y. Dai, X. Y. Qin and X. Y. Zhang, *ACS Appl. Mater. Interfaces*, 2013, **5**, 7654-7658.
7. M. Savage, S. Yang, M. Suyetin, E. Bichoutskaia, W. Lewis, A. J. Blake, S. A. Barnett and M. Schröder, *Chem. Eur. J.*, 2014, **20**, 8024-8029.
8. B. Panella, M. Hirscher, H. Putter and U. Muller, *Adv. Funct. Mater.*, 2006, **16**, 520-524.
9. X. Lin, G. Gao, L. Zheng, Y. Chi and G. Chen, *Anal. Chem.*, 2013, **86**, 1223-1228.
10. M. Zhang, G. Feng, Z. Song, Y.-P. Zhou, H.-Y. Chao, D. Yuan, T. T. Y. Tan, Z. Guo, Z. Hu, B. Z. Tang, B. Liu and D. Zhao, *J. Am. Chem. Soc.*, 2014, **136**, 7241-7244.
11. X. Zhang, F. X. Llabrés i Xamena and A. Corma, *J. Catal.*, 2009, **265**, 155-160.
12. J.-L. Wang, C. Wang and W. Lin, *Acs Catal.*, 2012, **2**, 2630-2640.
13. C. Wang, Z. Xie, K. E. deKrafft and W. Lin, *J. Am. Chem. Soc.*, 2011, **133**, 13445-13454.
14. D. Britt, H. Furukawa, B. Wang, T. G. Glover and O. M. Yaghi, *Proc. Natl. Acad. Sci. U.S.A.*, 2009, **106**, 20637-20640.
15. W. Wu, A. M. Kirillov, X. Yan, P. Zhou, W. Liu and Y. Tang, *Angew. Chem., Int. Ed.*, 2014, **126**, 10825-10829.
16. J. Yu, Y. Cui, C. Wu, Y. Yang, Z. Wang, M. O'Keeffe, B. Chen and G. Qian, *Angew. Chem., Int. Ed.*, 2012, **51**, 10542-10545.
17. J. Zou, Q. Peng, Z. Wen, G. Zeng, Q. Xing and G. Guo, *Cryst. Growth Des.*, 2010, **10**, 2613-2619.
18. J.-K. Sun and Q. Xu, *Energy Environ. Sci.*, 2014, **7**, 2071.
19. M. Y. Masoomi and A. Morsali, *Coord. Chem. Rev.*, 2012, **256**, 2921-2943.
20. C.-B. Li, Z.-J. Li, S. Yu, G.-X. Wang, F. Wang, Q.-Y. Meng, B. Chen, K. Feng, C.-H. Tung and L.-Z. Wu, *Energy Environ. Sci.*, 2013, **6**, 2597-2602.
21. F. Wang, W. J. Liang, J. X. Jian, C. B. Li, B. Chen, C. H. Tung and L. Z. Wu, *Angew. Chem., Int. Ed.*, 2013, **52**, 8134-8138.
22. X. Cheng, A. Zhang, K. Hou, M. Liu, Y. Wang, C. Song, G. Zhang and X. Guo, *Dalton Trans.*, 2013, **42**, 13698-13705.
23. N. V. Maksimchuk, K. A. Kovalenko, V. P. Fedin and O. A. Kholdeeva, *Chem. Commun.*, 2012, **48**, 6812-6814.
24. K. M. L. Taylor-Pashow, J. D. Rocca, Z. Xie, S. Tran and W. Lin, *J. Am. Chem. Soc.*, 2009, **131**, 14261-14263.
25. P. Wu, N. Du, H. Zhang, L. Jin and D. Yang, *Mater. Chem. Phys.*, 2010, **124**, 908-911.
26. M.-T. H. Nguyen and Q.-T. Nguyen, *J. Photochem. Photobiol., A*, 2014, **288**, 55-59.
27. C. Scherb, *Controlling the Surface Growth of Metal-Organic Frameworks*, Dissertation, LMU München, 2009.
28. R. M. Cornell and U. Schwertmann, *The Iron Oxides: Structure, Properties, Reactions, Occurrences and Uses*, Wiley-VCH, Second edn., 2003.
29. G. Tong, F. Du, L. Xiang, F. Liu, L. Mao and J. Guan, *Nanoscale*, 2014, **6**, 778-787.
30. D. L. A. d. Faria, S. V. Silva and M. T. d. Oliveira, *J. Raman Spectrosc.*, 1997, **28**, 873-878.
31. F. Zhang, H. Hu, H. Zhong, N. Yan and Q. Chen, *Dalton Trans.*, 2014, **43**, 6041.
32. T. Yu, Y. Zhu, X. Xu, K. S. Yeong, Z. Shen, P. Chen, C. T. Lim, J. T. Thong and C. H. Sow, *Small*, 2006, **2**, 80-84.
33. G. Gao, H. Wu, Y. Zhang, K. Wang, P. Huang, X. Zhang, S. Guo and D. Cui, *J. Mater. Chem.*, 2011, **21**, 12224.
34. Y. Liu, L. Yu, Y. Hu, C. Guo, F. Zhang and X. Wen Lou, *Nanoscale*, 2012, **4**, 183-187.
35. T. Fujii, F. M. F. d. Groot and G. A. Sawatzky, *Phys. Rev. B*, 1999, **59**, 3195-3202.
36. N. S. McIntyre and D. G. Zetaruk, *Anal. Chem.*, 1977, **49**, 1521-1529.
37. J.-D. Xiao, L.-G. Qiu, X. Jiang, Y.-J. Zhu, S. Ye and X. Jiang, *Carbon*, 2013, **59**, 372-382.
38. X. Wang, X. Chen, L. Gao, H. Zheng, M. Ji, C. Tang, T. Shen and Z. Zhang, *J. Mater. Chem.*, 2004, **14**, 905.
39. D. Li, X. Hu, Y. Sun, S. Su, A. Xia and H. Ge, *Rsc Adv.*, 2015, **5**, 27091-27096.
40. C. Y. Lee, O. K. Farha, B. J. Hong, A. A. Sarjeant, S. T. Nguyen and J. T. Hupp, *J. Am. Chem. Soc.*, 2011, **133**, 15858-15861.
41. A. Fateeva, P. A. Chater, C. P. Ireland, A. A. Tahir, Y. Z. Khimyak, P. V. Wiper, J. R. Darwent and M. J. Rosseinsky, *Angew. Chem. Int. Ed.*, 2012, **51**, 7440-7444.
42. X.-J. Yang, B. Chen, L.-Q. Zheng, L.-Z. Wu and C.-H. Tung, *Green Chem.*, 2014, **16**, 1082.
43. J. He, J. Wang, Y. Chen, J. Zhang, D. Duan, Y. Wang and Z. Yan, *Chem. Commun.*, 2014, **50**, 7063-7066.
44. J. Schneider, M. Matsuoka, M. Takeuchi, J. Zhang, Y. Horiuchi, M. Anpo and D. W. Bahnemann, *Chem. Rev.*, 2014, **114**, 9919-9986.
45. R. P. Sabatini, W. T. Eckenhoff, A. Orchard, K. R. Liwosz, M. R. Detty, D. F. Watson, D. W. McCamant and R. Eisenberg, *J Am Chem Soc*, 2014, **136**, 7740-7750.
46. M. P. McLaughlin, T. M. McCormick, R. Eisenberg and P. L. Holland, *Chem. Commun.*, 2011, **47**, 7989-7991.
47. J. Yang, D. Wang, H. Han and C. Li, *Acc. Chem. Res.*, 2013, **46**, 1900-1909.

48. C. Wang, K. E. deKrafft and W. Lin, *J. Am. Chem. Soc.*, 2012, **134**, 7211-7214.
49. S. Saha, G. Das, J. Thote and R. Banerjee, *J. Am. Chem. Soc.*, 2014, **136**, 14845-14851.
50. Y. Kataoka, K. Sato, Y. Miyazaki, K. Masuda, H. Tanaka, S. Naito and W. Mori, *Energy Environ. Sci.*, 2009, **2**, 397-400.
51. Y. Horiuchi, T. Toyao, M. Saito, K. Mochizuki, M. Iwata, H. Higashimura, M. Anpo and M. Matsuoka, *J. Phys. Chem. C*, 2012, **116**, 20848-20853.
52. G.-G. Luo, K. Fang, J.-H. Wu and J. Mo, *Chem. Commun.*, 2015, **51**, 12361-12364.
53. F. Wang, Y. Jiang, A. Gautam, Y. Li and R. Amal, *Acs Catalysis*, 2014, **4**, 1451-1457.
54. E. Joselevich and I. Willner, *J. Phys. Chem.* , 1995, **99**, 6903-6912.
55. S. Yu, Y. H. Kim, S. Y. Lee, H. D. Song and J. Yi, *Angew. Chem., Int. Ed.*, 2014, **53**, 11203-11207.
56. R. R. Yeredla and H. Xu, *Nanotechnology*, 2008, **19**, 055706.
57. A. Murphy, *Sol. Energy Mater. Sol. Cells*, 2007, **91**, 1326-1337.
58. R. López and R. Gómez, *J. Sol-Gel Sci. Technol.*, 2011, **61**, 1-7.
59. S. Min and G. Lu, *J. Phys. Chem. C* 2011, **115**, 13938-13945.

Graphical Abstract

One MOF-derived magnetic carbonaceous photocatalyst was prepared *in situ* and demonstrated highly efficient visible-light-driven hydrogen evolution without noble metal cocatalyst.